Figure S1, related to Figure 1

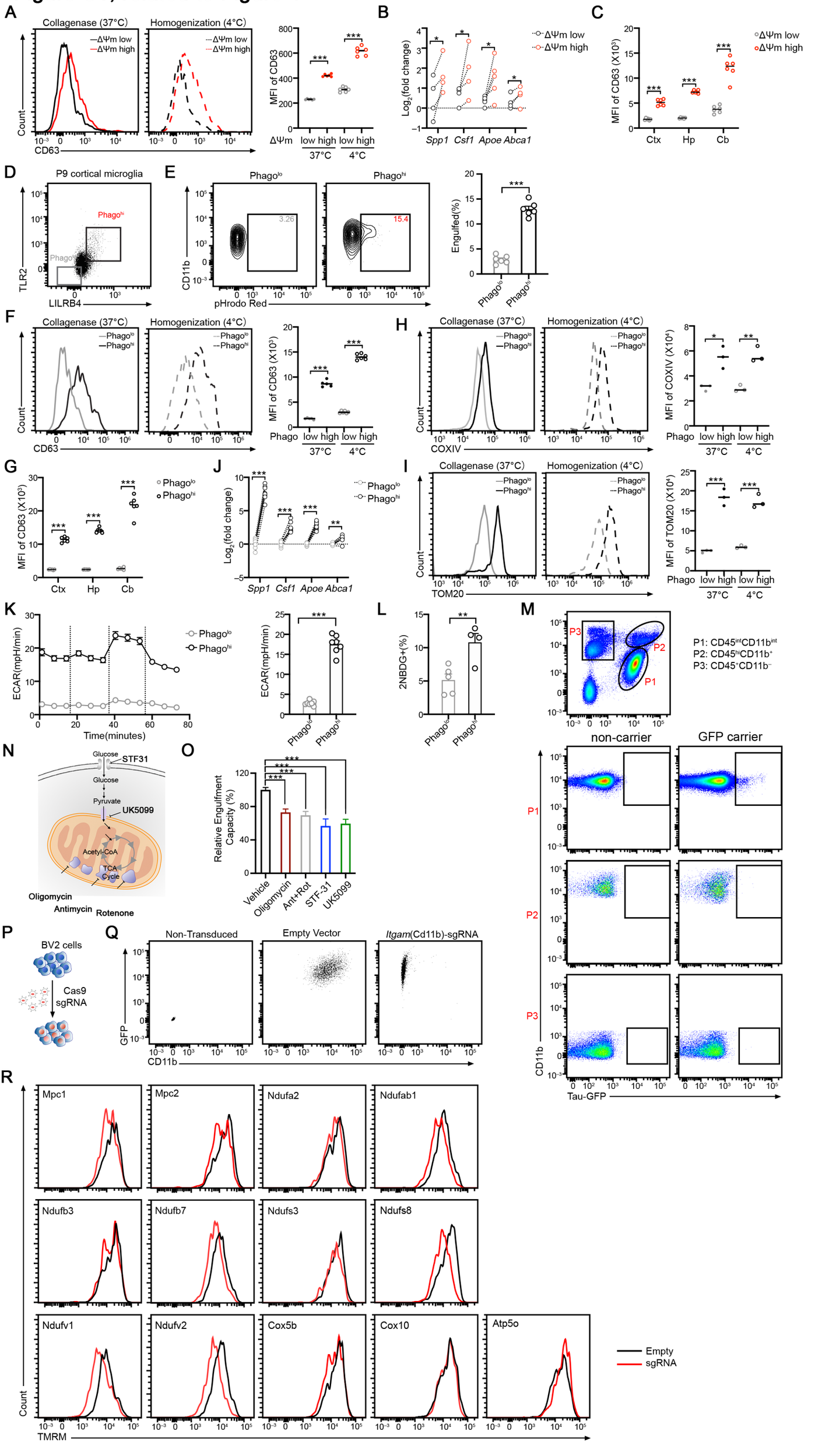

Figure S1. Related to Figure 1. Functional coupling between phagocytic activity and mitochondrial function in microglia.

(A) Representative FACS profiles and geometric mean fluorescence intensity of surface CD63 in indicated ΔΨm microglia subsets isolated by either Collagenase D dissociation or Dounce homogenization.

(B) Quantitative PCR analyses of selected genes in indicated ΔΨm microglia subsets isolated from P9 cortices by Dounce homogenization (n = 4 mice).

(C) Mean fluorescence intensity of surface CD63 staining analyzed by flow cytometry in indicated ΔΨm microglia subsets across different brain regions. Ctx: cortex; Hp: hippocampus; Cb: cerebellum (n = 6).

(D) Experimental strategy used for enrichment of Phago^{lo} (lower 10%) and Phago^{hi} (higher 10%) microglia subsets from P9 cortices based on relative expression levels of TLR2 and LILRB4 by flow cytometry.

(E) Validation of phagocytic capacity of indicated microglia subsets (n = 6).

(F) Representative FACS plots and geometric mean fluorescence intensity of surface CD63 staining in indicated Phago^{lo} and Phago^{hi} microglia subsets isolated by either Collagenase D dissociation or Dounce homogenization (n = 6).

(G) Mean fluorescence intensity of surface CD63 staining analyzed by flow cytometry in Phago^{lo} *vs* Phago^{hi} microglia subsets across different brain regions. Ctx: cortex; Hp: hippocampus; Cb: cerebellum (n = 6).

(H-I) Representative FACS plots and geometric mean fluorescence intensities of intracellular staining of COXIV(**H**) and TOM20 (**I**) in indicated Phago^{lo} and Phago^{hi} microglia subsets isolated by either Collagenase D dissociation or Dounce homogenization (n = 3).

(J) Quantitative PCR analyses of selected genes in Phago^{lo} *vs* Phago^{hi} microglia subsets (**H**) isolated from P9 cortices by Dounce homogenization (n = 8).

(K) Real-time changes in extracellular acidification rate (ECAR) of freshly sorted Phago^{lo} and Phago^{hi} microglia subsets in response to a Mito Stress test. ECAR is reported as milli-pH units (mpH) per minute (n = 7).

(L) Glucose uptake capacity in Phago^{lo} and Phago^{hi} microglia subsets as measured by proportion of cells labeled with fluorescently labeled 2-NBDG (Phago^{lo}: n = 5, Phago^{hi}: n = 4).

(M) Representative FACS profiles showing Tau-GFP signals in $CD45^{int}CD11b^{int}$, $CD45^{hi}CD11b^{+}$ and $CD45^{+}CD11b^{-}$ populations isolated from P10 cortices. Tau-GFP noncarrier was used as a negative control. Tau-GFP signals were only robustly detected in $CD45^{int}CD11b^{int}$ populations.

(N) An overview of bioenergetics pathway depicting inhibitors of glucose transporter (STF-31), mitochondria pyruvate carrier (UK5099), mitochondrial respiratory complex I (Rotenone), complex III (Antimycin A) and complex V (Oligomycin).

(O) Relative phagocytic activity of primary mouse microglia measured by the fraction of cells that have engulfed synaptosome under indicated conditions. Data is normalized to the mean value of the vehicle group (vehicle: $n = 20$, Oligomycin: $n = 12$, Antimycin+Retenone: $n = 9$, STF-31: $n = 9$, UK5099: $n = 5$; pooled from 3 experiments).

(P) Schematic displaying the experimental design for functional metabolic sgRNA studies.

(Q) Validation of CRISPR/Cas9 knockout efficiency. BV2 cells were lentivirally transduced with either Cas9-GFP-Guide only or Cas9-GFP-Guide-expressing sgRNAs against *Itgam* (CD11b). CD11b protein expression was measured by flow cytometry on day 7 after infection.

(R) Mitochondria membrane potential measured by TMRM staining in BV2 cells lentivirally transduced with either Cas9-GFP- only or Cas9-GFP-Guide-expressing sgRNAs against indicated metabolic enzymes or transporters.

Statistics: middle line: mean (**A**, **C**, **F**, **G**, **H** and **I**); mean ± SEM (**E**, **L** and **O**); mean ± SD (**K**); student's *t* test (**A-C** and **E-L**), one-way ANOVA test (**O**); *$p<0.05$, **$p<0.01$, ***$p<0.001$.

Figure S2, related to Figure 2

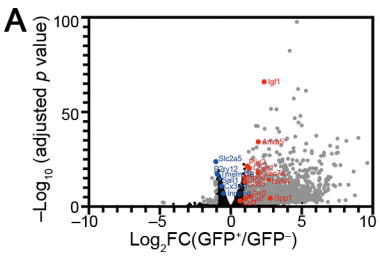

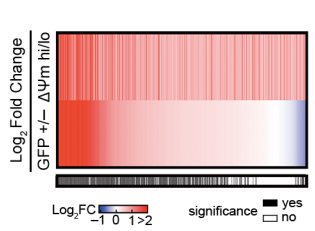

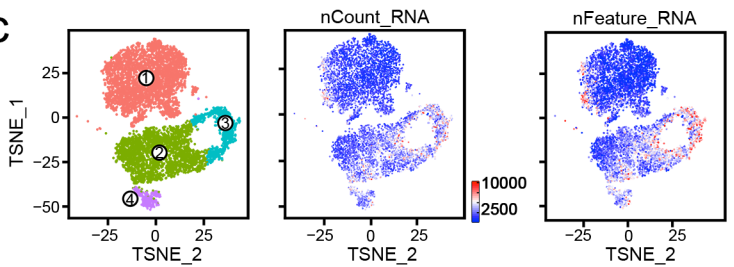

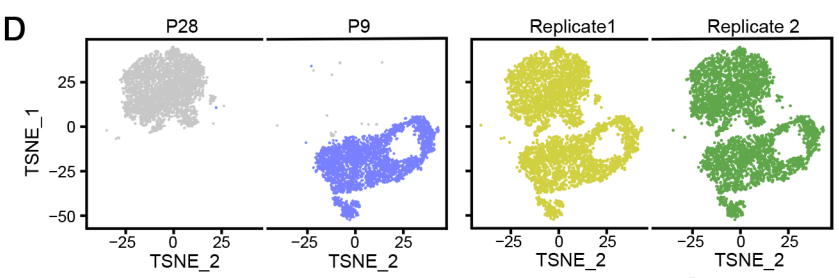

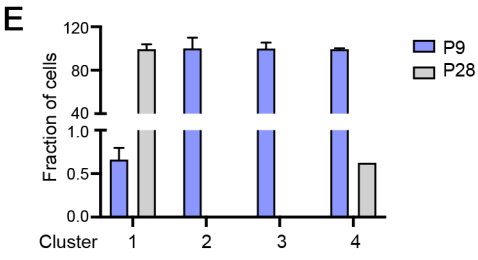

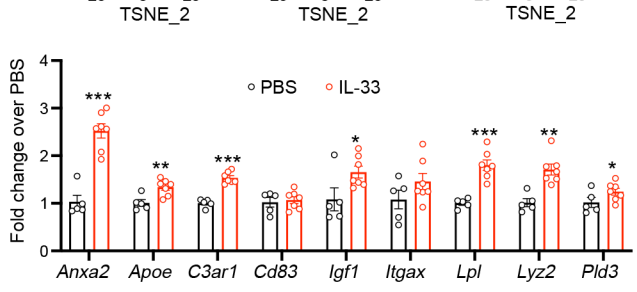

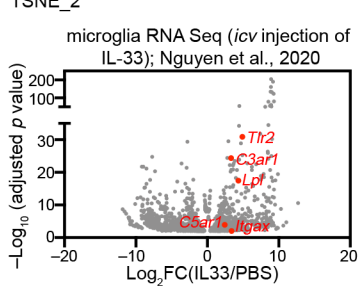

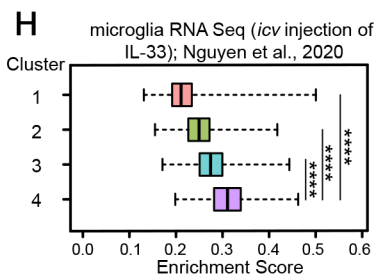

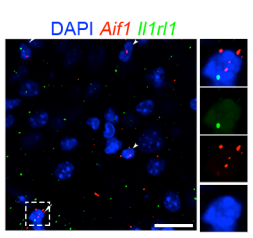

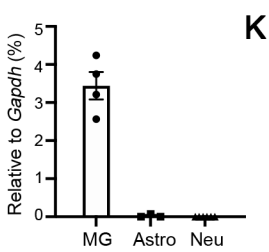

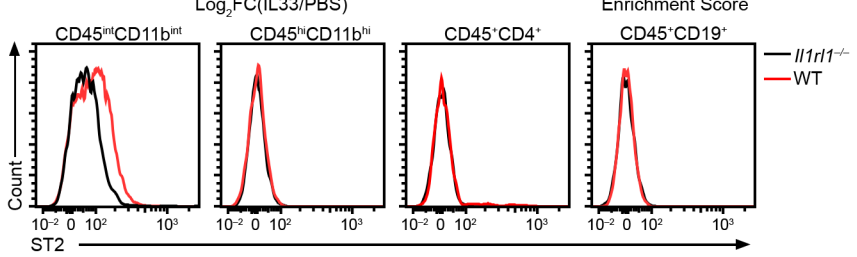

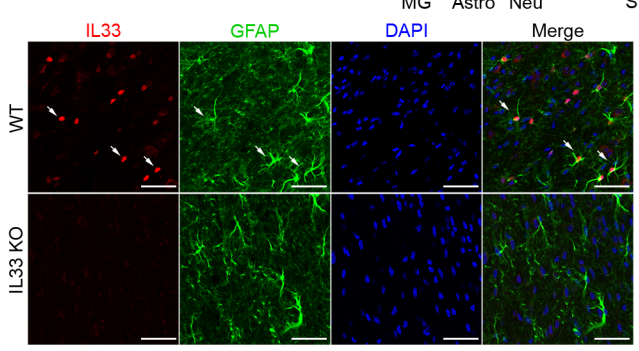

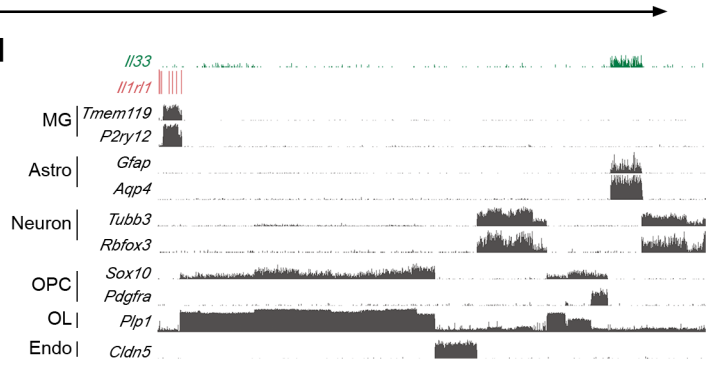

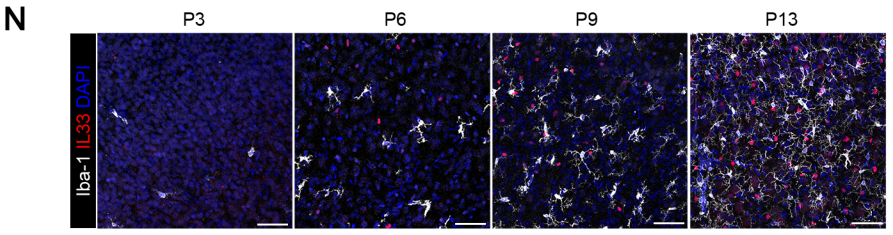

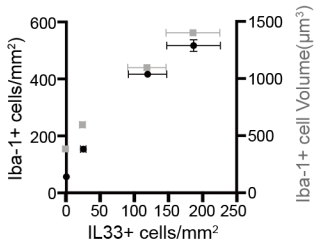

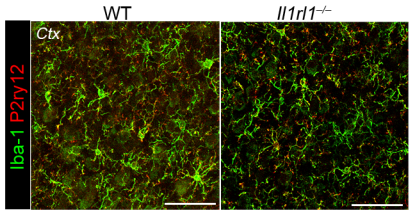

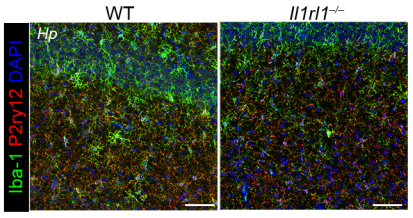

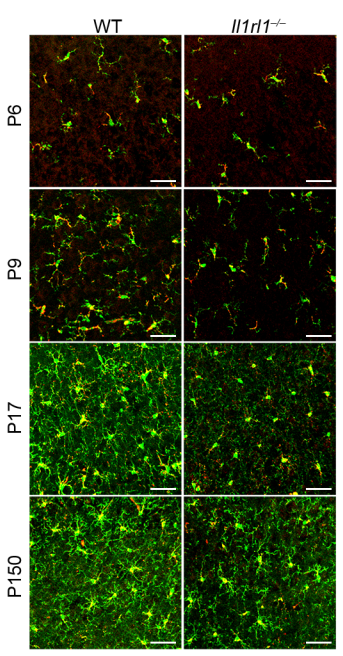

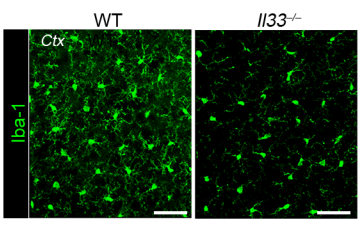

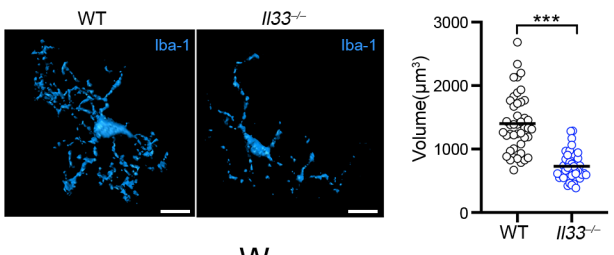

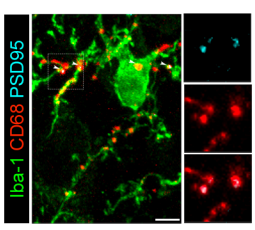

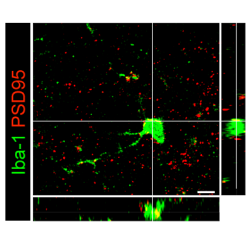

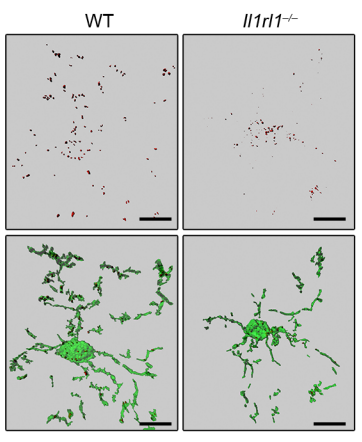

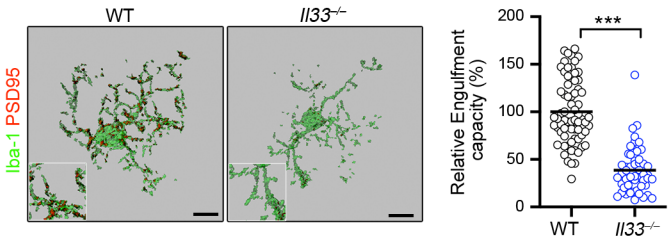

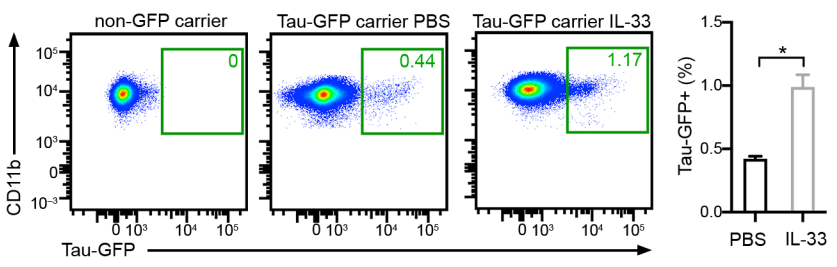

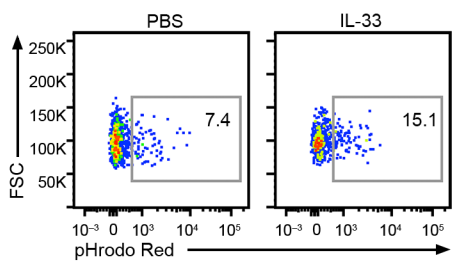

Figure S2. Related to Figure 2. *Il33/Il1rl1* deficiency leads to microglial malfunction and dysmorphology in the developing brain

(A) Volcano plot depicting genes enriched/depleted from Tau-GFP^{+} microglia (microglia engulfed neuronal materials) compared to Tau-GFP^{-} subsets. Selected genes are highlighted.

(B) Heatmap summarizing gene expression from RNA-seq results of TMRM^{hi} *vs* TMRM^{lo} and Tau-GFP^{+} *vs* Tau-GFP^{-} dataset. Log2(FoldChange) is plotted. Genes shown isTMRM signature (genes significantly upregulated in TMRM^{hi} microglia). Bottom color bar: significantly changed (black) or not (white) in Tau-GFP+ microglia.

(C-D) *t*-SNE visualizationof single-cell profiles (dots) from P9 and P28 microglia colored by *post hoc* annotation, number of RNA count, number of Feature RNA, age of the mice and replicates.

(E) Proportion of cells from P9 and P28 animals in the different clusters (n = 2).

(F) Quantitative PCR analyses of selected genes in cortical microglia isolated from PBS and IL-33 administered mice at postnatal day 9 (PBS: n = 5, IL-33: n = 7; representative of 2 experiments).

(G) Volcano plot of differentially expressed genes in hippocampal microglia after *i.c.v.* injection of IL-33. Data is from GSE150714.

(H) Distribution of IL-33 induced genes in the 4 clusters in (**C**). IL-33 induced genes are derived from GSE150714 shown in (**G**).

(I) Single-molecule hybridization chain reaction (*sm*HCR) of mRNA molecules *Il1rl1*(green) and *Aif1* (red), a pan-microglia/macrophage marker in the somatosensory cortex at P15. Nuclei were counterstained with DAPI (blue) (Scale bar = 20μm).

(J) Quantitative PCR analysis of *Il1rl1* in flow sorted microglia (MG), astrocyte (Astro) and neuron (Neu). Relative expression of *Il1rl1* is normalized to *Gapdh*. *Il1rl1* was only detected in microglia.

(K) Representative flow cytometry plots of ST2 staining on various immune populations from mouse brain, including microglia (CD45^{int}CD11b^{int}), monocyte/macrophage (CD45^{hi}CD11b^{hi}), T cells (CD45^{+}CD4^{+}) and B cells (CD45^{+}CD19^{+}). *Il1rl1*$^{-/-}$ cells were used as a negative control.

(L) Immunostaining for IL-33 (red) and astrocyte marker GFAP (green) in WT and *Il33*$^{-/-}$ KO brains. Nuclei were counterstained with DAPI (blue). Scale bar, 50μm.

(M) Plots displaying the incidence and amplitude of *Il1rl1*, *Il33* and selected lineage markers in various cell types in the mouse brain. *Il1rl1* was exclusively expressed by microglia but not non-myeloid brain cells, and *Il33* was predominantly expressed by astrocytes. Data from Linnarsson lab Mouse Brain Atlas (http://mousebrain.org/).

(N) Representative confocal image showing Iba-1 (white) and IL-33 (red) expression in the somatosensory cortex at indicated ages. Nuclei were counterstained with DAPI (blue). Scale bar, 50μm.

(O) Quantification of IL33-expressing cell density, Iba1-expressing cell density and microglia cellular volume in the somatosensory cortex at indicated ages.

(P-Q) Representative confocal images of Iba-1+ (green) and P2RY12+ (red) microglia in the somatosensory cortex (**P**) and hippocampus (**Q**) from *Il1rl1*$^{-/-}$ and control mice at P14 (Scale bar = 50μm).

(R) Representative confocal images of Iba-1 (green) and CD68 (red) staining in the somatosensory cortex from *Il1rl1*$^{-/-}$ and control mice at indicated ages (Scale bar = 50μm).

(S) Representative confocal images of Iba1+ microglia (green) in the somatosensory cortex from *Il33*$^{-/-}$ and control mice at P13 (Scale bar = 50μm).

(T) Representative 3D reconstructions of Iba1-stained microglia and quantification of cellular volume of individual microglia residing in somatosensory cortex of WT or *Il33*$^{-/-}$ mice at P13 (Scale bar = 10μm) (WT: $n = 71$, *Il33*$^{-/-}$ KO: $n = 53$; pooled from 4 mice/group).

(U) Confocal images of engulfed PSD-95 colocalizing with CD68+ lysosomes within microglia. Scale bar, 5μm.

(V) Orthogonal view of high-resolution confocal image shows colocalization of PSD-95 (red) and Iba-1 (green). Scale bar, 10μm.

(W) Three-dimensional reconstruction and surface rendering showing microglia (green, Iba1) and engulfed synaptic debris (red, CD95) in the somatosensory cortex of WT or *Il1rl1*$^{-/-}$ mice at P17 (Scale bar = 10μm).

(X) Representative three-dimensional reconstruction and surface rendering of microglia and quantification of microglia engulfment activity as measured by engulfed synaptic debris content within each microglia (surface rendered microglia (green, Iba1) and (red, CD95)) in cortex of WT or *Il33*$^{-/-}$ mice at P13 (Scale bar = 10μm) (WT: $n = 49$, *Il33*$^{-/-}$; pooled from 3-5 mice/group).

(Y) Flow cytometry plots and quantification showing the percentage of tau-GFP^{+} microglia out of total cortical microglia from mice injected with PBS or IL-33. Non-GFP carrier samples were used as negative control (PBS: $n = 2$, IL33: $n = 3$; representative of 2 experiments).

(Z) Representative FACS profiles of engulfed synaptosome intensity in microglia under indicated conditions.

Statistics: mean ± SEM (**E**, **F**, **J**, **O** and **Y**); middle line: mean, box edges: 25th and 75th percentiles, whiskers: extend to 5th to 95th percentile (**H**); middle line: mean (**T** and **X**); student's *t* test (**F**, **T**, **X** and **Y**); one-way ANOVA test (**H**); **p*<0.05, ***p*<0.01, ****p*<0.001， *****p* <10^{-12}.

Figure S3, related to Figure 3

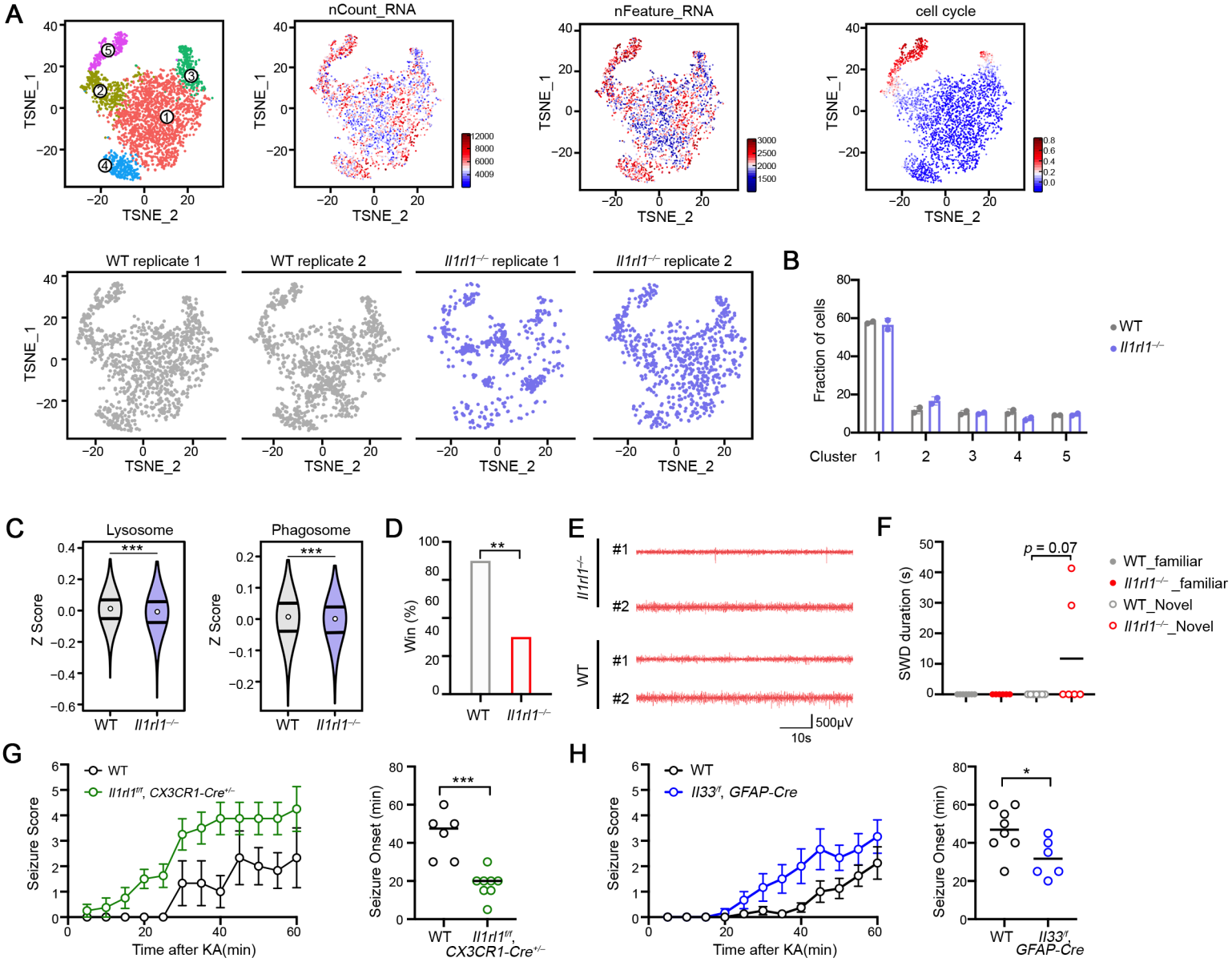

Figure S3. Related to Figure 3. *Il1rl1* deficiency leads to microglial dysfunction and behavioral abnormalities.

(A) *t*SNE plots showing WT and *Il1rl1*$^{-/-}$ microglia that are color-coded by assigned cluster number, number of RNA count, number of Feature RNA, cell cycle score, genotype and replicates.

(B) Proportion of microglial cells from WT and *Il1rl1*$^{-/-}$ mice in the different clusters.

(C) Violin plots showing distribution of lysosome and phagosome signature in WT and *Il1rl1*$^{-/-}$ microglia.

(D) Percentage of wins in test pairs between WT and *Il1rl1*$^{-/-}$ mice, 3/10 (30%) of *Il1rl1*$^{-/-}$ wins versus WT; *Il1rl1*$^{-/-}$ mice performed significantly below chance level.

(E) EEG recordings in *Il1rl1*$^{-/-}$ and WT mice housed in their home cages.

(F) SWD duration of WT and *Il1rl1*$^{-/-}$ mice housed in a familiar cage or placed into a new cage (WT: n =7, *Il1rl1*$^{-/-}$: n = 6).

(G-H) Seizure severity score following kainic acid administration in *Il1rl1*$^{f/f}$*::CX3CR1-Cre*$^{+/-}$ (**G**) or *Il33*$^{f/f}$*::GFAP-Cre* (**H**) versus WT mice at P28-P35. Onset of seizure is quantified as the bar graphs on the right (for (**G**), WT: n = 6, *Il1rl1*$^{f/f}$*::CX3CR1-Cre*$^{+/-}$: n = 8; for (**H**), WT: n = 8, *Il33*$^{f/f}$*::GFAP-Cre*: n = 6).

Statistics: circle: mean, lines: first and third quartiles (**C**); middle line: mean (**F** and **G-H**); mean ± SEM (**G-H**); Mann-Whitney test (**C**), one-sample *chi*-square test (**D**), one-way ANOVA test (**F**), student's *t* test (**G-H**); *p<0.05, **p<0.01, ***p<0.001.

Figure S4, related to Figure 4

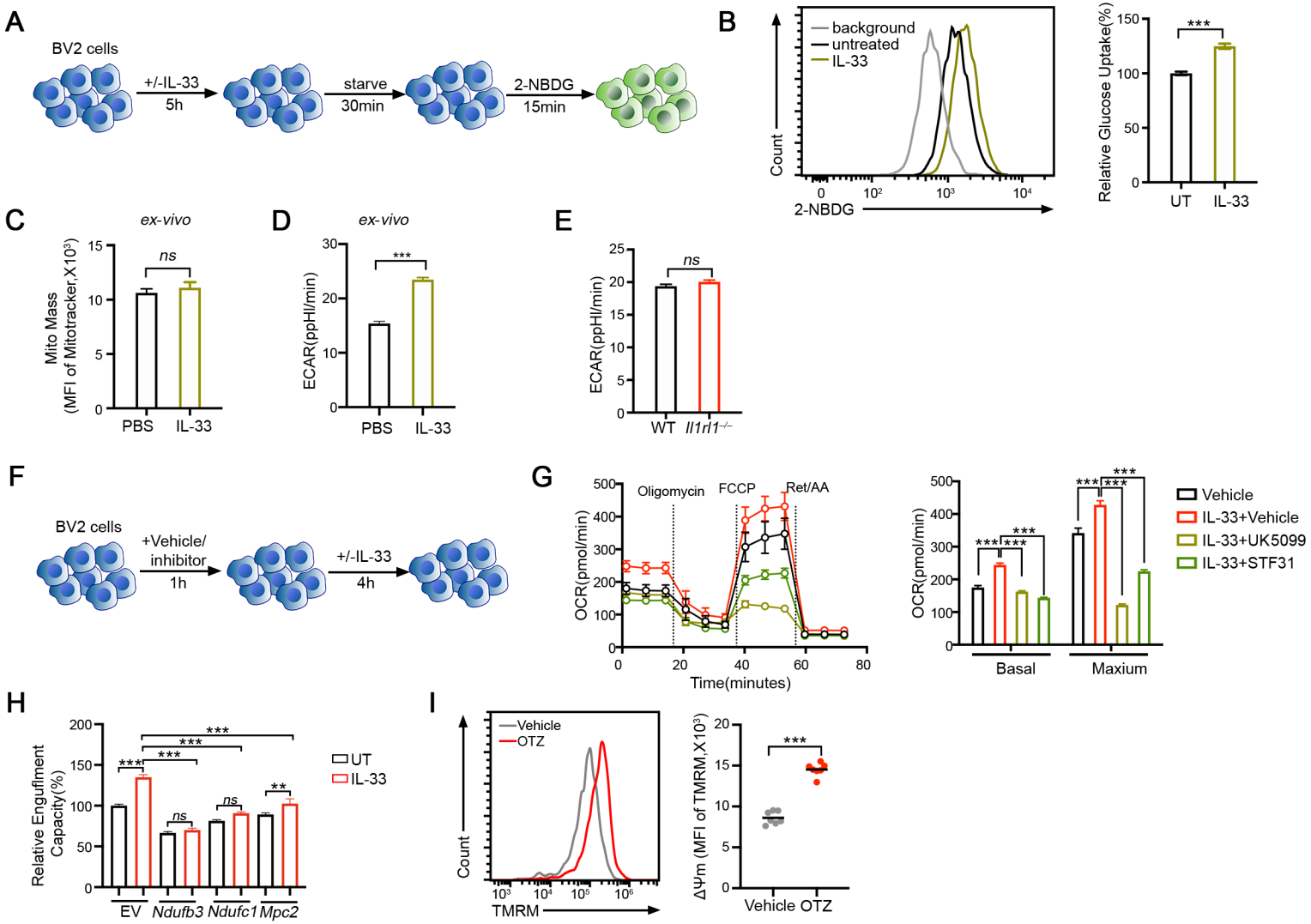

Figure S4. Related to 4. IL33 promotes microglial function via modulating metabolic activity.

(A) Schematic of the experimental design for the glucose uptake capacity studies *in vitro*.

(B) Representative FACS profiles of 2-NBDG intensity and quantification of 2-NBDG uptake capacity (geometric mean fluorescence intensity of 2-NBDG minus background intensity) in the presence or absence of IL-33 (UT: $n = 30$, IL-33: $n = 43$; pooled from 2 experiments).

(C) Mitochondrial mass quantified as the geometric mean fluorescence intensity of MitoTracker Green staining in microglia under indicated conditions (PBS: $n = 9$, IL-33: $n = 6$).

(D) Lactate release activity as measured by extracellular acidification rate (ECAR) of freshly sorted microglia from PBS and IL-33 administered mice at baseline ($n = 12$, representative of 2 experiments).

(E) Lactate release activity as measured by extracellular acidification rate (ECAR) of acutely isolated WT and *Il1rl1*$^{-/-}$ microglia at baseline ($n = 7$).

(F) Schematic of the experimental design for inhibitor studies *in vitro*.

(G) Mitochondrial function of BV2 cells under indicated conditions analyzed by Mito Stress test assay ($n = 10$).

(H) Engulfment capacity as measured by engulfed synaptosome intensity in BV2 cells transduced with sgRNAs targeting *Nudfb3*, *Ndufc1* and *MPc2*, in the presence or absence of IL-33 as indicated (EV: $n = 11$, EV + IL-33: $n = 11$, sg-*Ndufb3*: $n = 14$, sg-*Ndufb3*+IL-33: $n = 12$, sg-*Ndufc1*: $n = 14$, sg-*Ndufc1*+IL-33: $n = 13$, sg-*Mpc2*: $n = 14$, sg-*Mpc2*+IL-33: $n = 9$).

(I) Representative flow cytometry plots and geometric mean fluorescence intensities of and TMRM in primary rat microglia treated with DMSO (Vehicle) or Oltipraz (OTZ) for 12hrs ($n = 7$).

Statistics: mean ± SEM (**B**, **C** and **H**); mean ± SD (**D**, **E** and **G**); middle line: mean (**I**); student's *t* test (**B-E** and **I**), one-way ANOVA test (**G** and **H**); *ns*: not significant, $^{**}p<0.01$, $^{***}p<0.001$.

Figure S5,related to Figure 5

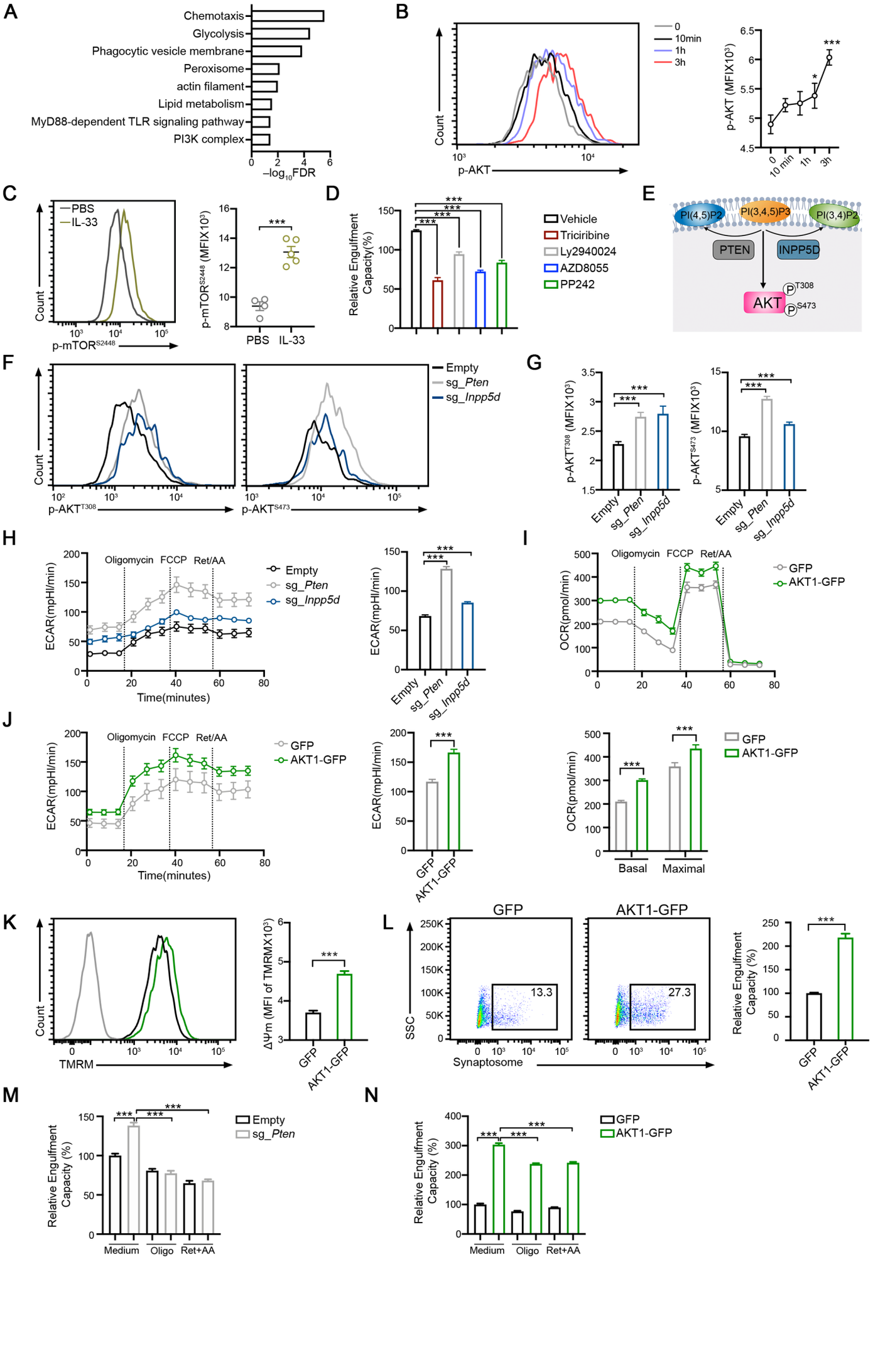

Figure S5. Related to Figure 5. AKT promotes mitochondrial bioenergetics and engulfment capacity

(A) Top enriched GO terms from genes that are induced by IL-33 in primary microglia. FDR: false discovery rate.

(B) Representative flow cytometry profiles showing intracellular staining of phosphorylated AKT in BV2 cells stimulated with IL-33 at indicated time points. The total amount of phosphor-AKT as shown by MFI is plotted in the graph on the right (n = 4).

(C) Representative flow cytometry plots and geometric mean fluorescence intensity of p-mTOR^{S2448} in cortical microglia isolated from PBS and IL-33 administered mice at postnatal day 9 (n = 4-5 mice/condition).

(D) Relative phagocytic activity of BV2 cells measured by the fraction of cells that have engulfed synaptosome under indicated conditions (vehicle: n = 27, Triciribine: n = 27, Ly294002: n = 18, AZD 8055: n = 9, PP242: n = 27; pooled from 7 experiments).

(E) An overview of AKT phosphorylation negatively-regulated by PTEN and SHP1 (INPP5D).

(F) Representative FACS profiles showing intracellular staining of phosphorylated AKT (T308) and phosphorylated AKT (S473) in BV2 cells transduced with sgRNAs targeting *Inpp5d* and *Pten*.

(G) Bar graph depicting the total amount of phosphor-AKT as shown by geometric mean fluorescence intensities in BV2 cells transduced with sgRNAs targeting *Inpp5d* and *Pten* (Empty: n = 10, sg-*Pten*: n = 7, sg-*Inpp5d*: n = 7).

(H) Lactate release activity as measured by extracellular acidification rate (ECAR) of BV2 cells transduced with sgRNAs targeting *Inpp5d* and *Pten* analyzed at baseline and following sequential treatment with oligomycin, FCCP, and rotenone + antimycin. Baseline ECAR is plotted as bar graph on the right (Empty: n = 8, sg-*Pten*: n = 11, sg-*Inpp5d*: n = 11; representative of 2 experiments).

(I) Mitochondrial function of BV2 cells transduced with GFP-expressing or AKT1-GFP expressing viruses, analyzed by Mito Stress test assay (GFP: n = 13, AKT1-GFP: n = 11; representative of 2 experiments).

(J) Lactate release activity as measured by extracellular acidification rate (ECAR) of BV2 cells transduced with GFP-expressing or AKT1-GFP expressing viruses analyzed at baseline and following sequential treatment with oligomycin, FCCP, and rotenone + antimycin. Baseline ECAR

is plotted as bar graph on the right (GFP: n = 13, AKT1-GFP: n = 11; representative of 2 experiments).

(K) Mitochondria membrane potential measured by TMRM staining in BV2 cells transduced with GFP-expressing or AKT1-GFP expressing viruses (n = 11, representative of 3 experiments).

(L) Representative flow cytometry profiles of engulfed synaptosome intensity BV2 cells transduced with GFP-expressing or AKT1-GFP expressing viruses. Relative proportion of cells positive for synaptosome is quantified in the bar graph on the right (GFP: n = 36, AKT1-GFP: n = 44; pooled from 3 experiment).

(M-N) Relative phagocytic activity of BV2 cells measured by engulfed synaptosome intensity under indicated conditions. Cells expressing sgRNAs targeting *Pten* (**M**) and cells overexpressing AKT (**N**) showed enhanced phagocytic ability and mitochondrial inhibition abrogated the effect (Empty + medium: n = 22, sg_*Pten* + medium: n = 22, Empty + Oligomycin: n = 21, sg_*Pten* + Oligomycin: n = 22, Empty + Ret/AA: n = 22, sg_*Pten* + Ret/AA: n = 22, lenti-GFP + medium: n = 11, lenti-GFP-AKT + medium: n = 22, lenti-GFP + Oligomycin: n = 11, lenti-GFP-AKT + Oligomycin: n = 22, lenti-GFP + Ret/AA: n = 10, lenti-GFP-AKT + Ret/AA: n = 21; pooled from 2 experiments).

Statistics: mean ± SEM (**B**, **C**, **D**, **G** and **K-N**), mean ± SD (**H-J**); one-way ANOVA test (**B**, **D**, **G**, **H**, **M** and **N**), student's t test (**C**, **I**, and **J-L**); *p<0.05, ***p<0.001.

Figure S6, related to Figure 6

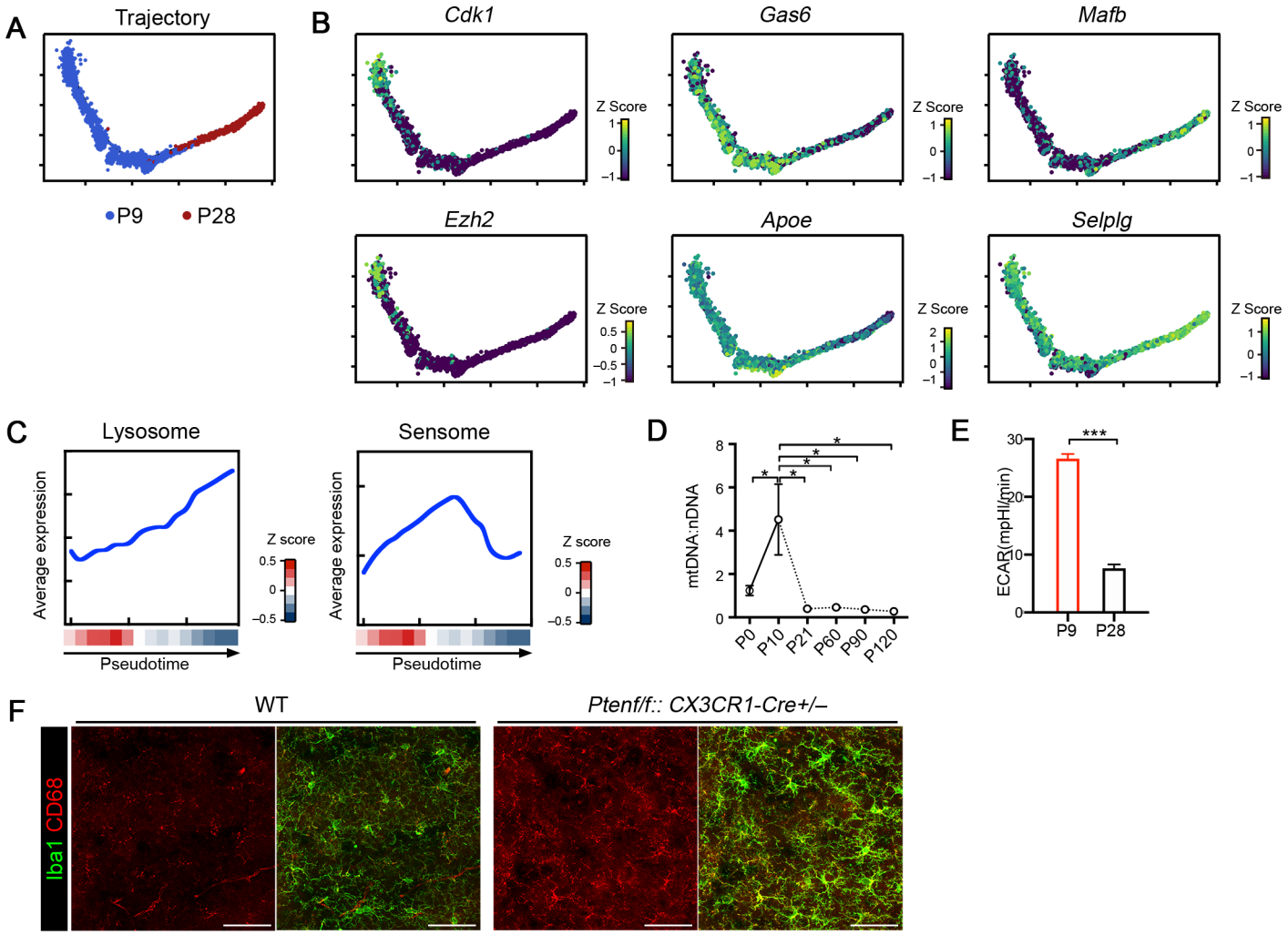

Figure S6. Related to Figure 6. Metabolic remodeling adapts to functional shifting in microglia during neurodevelopment.

(A) Dimensionality-reduction and pseudo-time ordering of the microglia isolated from P9 and P28 cortices. Individual points correspond to single cells colored by age. Arrow indicates direction of trajectory inferred from the expression of most dispersed genes across single cells.

(B) Relative expression of canonical microglial development marker genes along the inferred trajectory. Markers: *Cdk1*, *Ezh2* (early-microglia), *Gas6*, *Apoe* (pre-microglia), *Mafb* and *Selplg* (adult microglia).

(C) Average expression of genes involved in indicated gene signature or GO term along the pseudotemporal trajectory. Curve reflects a LOESS fit of single cell expression; color bar indicates relative expression along pseudo-time. Sensome: genes constituting microglial sensing apparatus; Lysosome: lysosome organization, GO:0007040.

(D) Mitochondrial mass of microglia at various ages assessed by the ratio of mitochondrial-to nuclear DNA (P0:$n = 5$, P9: $n = 6$, P12: $n = 4$, P60: $n = 3$, P90: $n = 3$, P120: $n = 3$).

(E) Lactate release activity as measured by extracellular acidification rate (ECAR) of P9 and P28 microglia analyzed by seahorse assay. Baseline ECAR is shown (P9: $n = 10$, P28: $n = 15$).

(F) Representative images of cortical microglia stained with the lysosomal marker CD68 (red) and the microglia/macrophage marker (Iba-1) from WT and *Pten*$^{f/f}$*:: CX3CR1-Cre*$^{+/-}$ mice at P28 (Scale bar = 50μm).

Statistics: mean ± SEM (**D**), mean ± SD (**E**); one-way ANOVA test (**D**), student's *t* test (**E**); **p*<0.05, ****p*<0.001.